

# Efficient Transformed Gaussian Process State-Space Models for Non-Stationary High-Dimensional Dynamical Systems

Zhidi Lin<sup>✉</sup>, Ying Li, Feng Yin<sup>✉</sup>, *Senior Member, IEEE*, Juan Maroñas<sup>✉</sup>, and Alexandre H. Thiéry<sup>✉</sup>

**Abstract**—Gaussian process state-space models (GPSSMs) have emerged as a powerful framework for modeling dynamical systems, offering interpretable uncertainty quantification and inherent regularization. However, existing GPSSMs face significant challenges in handling high-dimensional, non-stationary systems due to computational inefficiencies, limited scalability, and restrictive stationarity assumptions. In this paper, we propose an efficient transformed Gaussian process state-space model (ETGPSSM) to address these limitations. Our approach leverages a single shared Gaussian process (GP) combined with normalizing flows and Bayesian neural networks, enabling efficient modeling of complex, high-dimensional state transitions while preserving scalability. To address the lack of closed-form expressions for the implicit process in the transformed GP, we follow its generative process and introduce an efficient variational inference algorithm, aided by the ensemble Kalman filter (EnKF), to enable computationally tractable learning and inference. Extensive empirical evaluations on synthetic and real-world datasets demonstrate the superior performance of our ETGPSSM in system dynamics learning, high-dimensional state estimation, and time-series forecasting, outperforming existing GPSSMs and neural network-based methods in both accuracy and computational efficiency.

**Index Terms**—Gaussian process, high-dimensional data, state-space model, normalizing flow, Bayesian neural network, non-stationary dynamics.

## I. INTRODUCTION

STATE-SPACE models (SSMs) offer a versatile framework for capturing dynamical systems where latent states evolve based on internal dynamics and external inputs [1]. For systems with well-defined dynamics, Bayesian filtering methods—including the Kalman filter (KF), extended Kalman filter (EKF), ensemble Kalman filter (EnKF), and particle filter (PF)—enable sequential state estimation by integrating prior knowledge with new observations, thus facilitating reliable predictions in uncertain conditions. This capability makes

SSMs highly applicable in fields such as robotics, finance, control systems, and signal processing, where modeling temporal dependencies is essential [2], [3], [4]. Yet, in many complex real-world scenarios, the lack of precise knowledge about system dynamics significantly limits traditional SSM methods, particularly for nonlinear, high-dimensional systems like climate models, physiological processes, robotics, and neural dynamics [5], [6].

To address this challenge, numerous data-driven modeling and system identification approaches have been proposed. Deterministic models, such as deep state-space models (DSSMs), employ neural networks to learn system dynamics and have gained popularity for their ability to capture high-dimensional, nonlinear behaviors [7]. However, these models often demand extensive training datasets to mitigate overfitting, exhibit limited generalization in uncertain environments, and lack interpretability in their predictions [8], [9]. Consequently, despite their theoretical potential, DSSMs frequently underperform in practical applications.

In contrast, stochastic models incorporating flexible random process priors offer a robust alternative within a Bayesian learning framework [10]. A prominent example is Gaussian process state-space models (GPSSMs), which utilize Gaussian processes (GPs) to provide interpretable uncertainty quantification and inherent regularization, making them particularly advantageous for modeling safety-critical dynamical systems [11], [12]. Consequently, GPSSMs have been extensively utilized in various applications, including human pose and motion learning [13], robotics and control learning [14], reinforcement learning [15], [16], target tracking and navigation [17], and magnetic-field sensing [18].

Research on GPSSMs has also focused on advancing learning and inference methodologies. Early work either assumed a pre-learned GPSSM and concentrated solely on latent state inference—an impractical assumption for many real-world applications [19], [20], [21]—or employed maximum a posteriori (MAP) estimation to jointly infer the model and latent states [13], [22], which is computationally expensive and prone to overfitting. To address this issue, a significant advancement came with the introduction of a fully Bayesian treatment of GPSSMs using particle Markov chain Monte Carlo (PMCMC) [23], though its computational cost remains prohibitive for long, high-dimensional trajectories. Subsequent efforts [24], [25], [26], [27] adopted reduced-rank GP approximations [28] to alleviate computational demands, yet PMCMC scalability

Zhidi Lin and Alexandre H. Thiéry are with the the Department of Statistics and Data Science, National University of Singapore, Singapore 117546 (e-mail: [zhidilin@nus.edu.sg](mailto:zhidilin@nus.edu.sg), [a.h.thiery@nus.edu.sg](mailto:a.h.thiery@nus.edu.sg)). Alexandre H. Thiéry is the corresponding author.

Ying Li is with the Department of Statistics and Actuarial Science, University of Hong Kong, Hong Kong, SAR, China (e-mail: [lynnli98@connect.hku.hk](mailto:lynnli98@connect.hku.hk)).

Feng Yin is with the School of Science and Engineering, The Chinese University of Hong Kong, Shenzhen, Shenzhen 518172, China (e-mail: [yinfeng@cuhk.edu.cn](mailto:yinfeng@cuhk.edu.cn)).

Juan Maroñas is with the Machine Learning Group, Universidad Autónoma de Madrid, and with the Department of Quantitative Methods at CUNEF University (e-mail: [juan.maronas@cunef.edu](mailto:juan.maronas@cunef.edu)).

remains a challenge. This has led to a growing interest in variational inference methods [12], [29], [30], [31], [32], [33], [34], [35], [36], [37], [38], [39], [40], [41], which leverage sparse GP approximations with inducing points to enhance scalability [42], [43].

Nevertheless, existing variational GPSSMs still suffer from significant challenges when modeling high-dimensional state spaces. The primary challenge is scalability: the cubic computational complexity of the GP model scales linearly with state dimensionality, while the parameter count grows quadratically, leading to inefficiencies in high-dimensional contexts [40]. Furthermore, most models neglect dependencies among the multidimensional outputs of the state transition function, resulting in model mismatch, loss of inductive bias, and reduced generalization, particularly when latent states are partially observed [41]. Additionally, the prevalent use of stationary GP priors for system dynamics often fails to capture time-varying and complex transition functions [39]. These constraints significantly hinder the ability of GPSSMs to accurately represent complex dynamic systems.

To address these challenges, this paper proposes a novel approach for learning and inference in GPSSMs tailored to non-stationary, high-dimensional dynamical systems. The primary contribution is the development and integration of an efficient yet flexible implicit process prior for the state transition function [44]. This prior combines the strengths of GPs, normalizing flows [45], and (Bayesian) neural networks, significantly enhancing modeling capabilities in high-dimensional state spaces. Our key contributions are summarized as follows:

- Instead of using multiple independent GPs for the transition function, we introduce an implicit random process called transformed GP that integrates a shared GP with normalizing flows, whose parameters are amortizedly learned by neural networks. This design enables efficient, flexible, and output-dependent modeling of high-dimensional state transitions while mitigating the computational and parameter complexity of traditional GPSSMs. Moreover, it effectively captures complex, time-varying transition functions that conventional stationary GP priors cannot represent.
- For model inference, we develop a scalable variational inference algorithm that approximates the posterior distribution of the transformed GP by following its generative process, addressing the computational challenges of implicit processes lacking explicit expressions. Additionally, we integrate the EnKF into the variational inference framework for efficient latent state estimation, ensuring robust performance while significantly reducing computational burden.
- Finally, various empirical evaluations in system dynamics learning, high-dimensional latent state estimation, and time-series prediction demonstrate the superior performance and efficiency of our approach. Notably, the proposed method not only improves efficiency compared to existing GPSSMs but also exhibits superior learning and inference performance compared to pure neural network-based methods.

The remainder of this paper is organized as follows. Section II presents preliminaries related to state-space models and discusses the issues in existing works. In Section III, we detail our proposed efficient SSM modeling approach for dynamical systems with high-dimensional state spaces, along with the associated variational inference algorithms. Section IV presents the experimental results, and we conclude this paper in Section V. Technical proofs, derivations, and supporting results are provided in the Appendix.

## II. PRELIMINARIES

In Section II-A, we introduce the SSM considered in this paper, followed by a briefly review of Gaussian process state-space model in Section II-B.

### A. State-Space Models (SSMs)

A generic SSM describes the probabilistic relationship between the latent state  $\mathbf{x}_t \in \mathbb{R}^{d_x} \subseteq \mathcal{X}$  and the observation  $\mathbf{y}_t \in \mathbb{R}^{d_y} \subseteq \mathcal{Y}$ . It can be mathematically expressed as:

$$\text{transition: } \mathbf{x}_{t+1} = \mathbf{f}(\mathbf{x}_t) + \mathbf{v}_t, \quad \mathbf{v}_t \sim \mathcal{N}(\mathbf{0}, \mathbf{Q}), \quad (1a)$$

$$\text{emission: } \mathbf{y}_t = \mathbf{C}\mathbf{x}_t + \mathbf{e}_t, \quad \mathbf{e}_t \sim \mathcal{N}(\mathbf{0}, \mathbf{R}). \quad (1b)$$

Here, the latent states follow a Markov process, meaning that at any time step  $t \in \mathbb{N}$ , the next state  $\mathbf{x}_{t+1}$  depends only on the current state  $\mathbf{x}_t$  and the transition function  $\mathbf{f}(\cdot) : \mathbb{R}^{d_x} \mapsto \mathbb{R}^{d_x}$ . In this paper, the emission function is assumed to be linear, with the coefficient matrix  $\mathbf{C} \in \mathbb{R}^{d_y \times d_x}$ . For systems with nonlinear emission functions, the latent state can be augmented to a higher dimension, transforming the system into one with a linear emission function, which mitigates the non-identifiability issues commonly encountered in data-driven SSMs [38], [12]. Both the latent states and observations are assumed to be perturbed by zero-mean Gaussian noise, with covariance matrices  $\mathbf{Q}$  and  $\mathbf{R}$ , respectively.

### B. Gaussian Process State-Space Models (GPSSMs)

As discussed in Section I, system dynamics in real-world complex scenarios are often unknown, with only noisy observations,  $\mathbf{y}_{1:T} = \{\mathbf{y}_t\}_{t=1}^T$ , available. Consequently, there has been growing interest in adopting data-driven approaches, such as Gaussian processes [11], to model these dynamics and capture the underlying uncertainties.

1) **Gaussian process (GP)**: The GP is a generalization of the Gaussian distribution over infinite index sets, enabling the specification of distributions over functions  $\tilde{f}(\cdot) : \mathbb{R}^{d_x} \mapsto \mathbb{R}$ . A GP is fully characterized by its mean function, often set to zero, and its covariance (kernel) function  $k(\mathbf{x}, \mathbf{x}')$ , which includes a set of hyperparameters  $\theta_{gp}$  that need to be optimized for model selection [11]. According to the definition of a GP, the function values  $\tilde{\mathbf{f}} = \{\tilde{f}(\mathbf{x}_i)\}_{i=1}^N \in \mathbb{R}^N$  at any finite set of points  $\mathbf{X} = \{\mathbf{x}_i\}_{i=1}^N \in \mathbb{R}^{N \times d_x}$  follow a joint Gaussian distribution, i.e.,

$$\tilde{\mathbf{f}} \mid \mathbf{X} = \mathcal{N}(\tilde{\mathbf{f}} \mid \mathbf{0}, \mathbf{K}), \quad (2)$$

where  $\mathbf{K} \in \mathbb{R}^{N \times N}$  is the covariance matrix evaluated on the finite input  $\mathbf{X}$  with  $[\mathbf{K}]_{i,j} = k(\mathbf{x}_i, \mathbf{x}_j)$ .

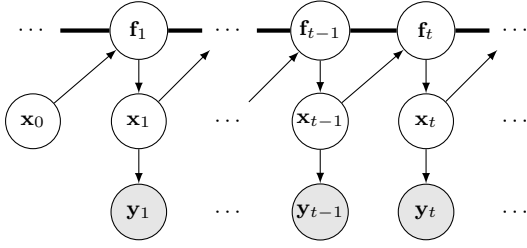


Fig. 1: Graphical model of GPSSM. The white circles represent the latent variables, while the gray circles represent the observable variables. The thick horizontal bar represents a set of fully connected nodes, i.e., the GP.

Given the observed function values  $\tilde{\mathbf{f}}$  at the input  $\mathbf{X}$ , the GP prediction distribution,  $p(\tilde{f}(\mathbf{x}_*)|\tilde{\mathbf{f}}, \mathbf{X})$ , at any new input  $\mathbf{x}_*$ , is Gaussian, fully characterized by the posterior mean  $\xi(\mathbf{x}_*)$  and the posterior variance  $\Xi(\mathbf{x}_*)$ . Concretely,

$$\xi(\mathbf{x}_*) = \mathbf{K}_{\mathbf{x}_*, \mathbf{X}} \mathbf{K}^{-1} \tilde{\mathbf{f}}, \quad (3a)$$

$$\Xi(\mathbf{x}_*) = k(\mathbf{x}_*, \mathbf{x}_*) - \mathbf{K}_{\mathbf{x}_*, \mathbf{X}} \mathbf{K}^{-1} \mathbf{K}_{\mathbf{X}, \mathbf{x}_*}^\top, \quad (3b)$$

where  $\mathbf{K}_{\mathbf{x}_*, \mathbf{X}}$  is the cross covariance matrix evaluated on the new input  $\mathbf{x}_*$  and the observed input  $\mathbf{X}$ .

2) **Gaussian process state-space model:** Placing a GP prior over the transition function  $\mathbf{f}(\cdot)$  in the classic SSM (see Eq. (1)) leads to the following salient GPSSM [12]:

$$\mathbf{f}(\cdot) \sim \mathcal{GP}(\mathbf{0}, k(\cdot, \cdot)), \quad (4a)$$

$$\mathbf{f}_t = \mathbf{f}(\mathbf{x}_{t-1}), \quad (4b)$$

$$\mathbf{x}_0 \sim p(\mathbf{x}_0), \quad (4c)$$

$$\mathbf{x}_t | \mathbf{f}_t \sim \mathcal{N}(\mathbf{x}_t | \mathbf{f}_t, \mathbf{Q}), \quad (4d)$$

$$\mathbf{y}_t | \mathbf{x}_t \sim \mathcal{N}(\mathbf{y}_t | \mathbf{C}\mathbf{x}_t, \mathbf{R}), \quad (4e)$$

where the initial state prior distribution  $p(\mathbf{x}_0)$  is assumed to be known and follows a Gaussian distribution. The graphical representation is depicted in Fig. 1.

In GPSSMs, when the state dimension  $d_x > 1$ , the transition  $\mathbf{f}(\cdot) : \mathbb{R}^{d_x} \mapsto \mathbb{R}^{d_x}$  is typically modeled using  $d_x$  mutually independent GPs. Each independent GP represents a dimension-specific function  $\mathbf{f}_d(\cdot) : \mathbb{R}^{d_x} \mapsto \mathbb{R}$ , and the multivariate output is expressed as

$$\mathbf{f}_t = \mathbf{f}(\mathbf{x}_{t-1}) = \{\mathbf{f}_d(\mathbf{x}_{t-1})\}_{d=1}^{d_x} = \{\mathbf{f}_{t,d}\}_{d=1}^{d_x}, \quad (5)$$

where each independent GP is characterized by a distinct kernel function and associated hyperparameters. The main challenge in GPSSMs is the simultaneous learning of the transition function and noise parameters, i.e., learning  $[\theta_{gp}, \mathbf{Q}, \mathbf{R}]$ , while inferring both the GPs and the latent states of interest.

3) **Challenges in high-dimensional state spaces:** While GPs offer modeling flexibility and a principled approach to quantifying uncertainty, they also introduce significant computational and modeling challenges.

- Modeling each latent state dimension with a separate GP results in a computational complexity of  $\mathcal{O}(d_x m^3)$ , where the complexity grows linearly with the dimensionality  $d_x$ . Here,  $m$  represents the number of samples, such as inducing points in sparse GP methods, used to compute

the GP kernel matrix. [11], [42], [43].

- When employing inducing point-based sparse GPs—a prevalent method—to variationally infer the posterior of the GP transition function in GPSSMs, the number of variational parameters grows quadratically with the state dimension. Specifically, the variational parameters include inducing inputs  $\mathbf{Z} \in \mathbb{R}^{d_x \times (m \times d_x)}$ , variational means  $\mathbf{M} \in \mathbb{R}^{d_x \times m}$ , and covariances  $\Sigma \in \mathbb{R}^{d_x \times (m \times m)}$  for the inducing outputs  $\mathbf{U} \sim \mathcal{N}(\mathbf{U} | \mathbf{M}, \Sigma)$ . As the state dimension increases, the quadratic scaling of  $\mathbf{Z}$  can render computations infeasible, while the scaling of  $\mathbf{M}$  and  $\Sigma$  further exacerbates the computational burden [40].
- The use of independent GPs for each dimension of the transition function simplifies the model but overlooks dependencies between outputs. This independence assumption can lead to model mismatch, reduced inductive bias, and ultimately degrade generalization and inference performance [46], [41].
- Existing GPSSMs commonly place a stationary GP prior over the transition function, as shown in Eq. (4a), to model a time-invariant transition function. However, this approach may fail to adequately capture non-stationary dynamics, leading to inaccuracies in scenarios where the transition function evolves over time.

Addressing these computational and modeling challenges is critical for enabling the practical application of GPSSMs in high-dimensional scenarios. In the next section, we detail our proposed method to resolve these issues.

### III. EFFICIENT TRANSFORMED GAUSSIAN PROCESS STATE-SPACE MODELS

We first present the proposed efficient and flexible modeling approach for high-dimensional state spaces in Section III-A. Subsequently, an efficient Bayesian variational inference is proposed in Section III-B, followed by the numerical evaluation details for the variational inference in Section III-C.

#### A. Efficient Modeling for High-Dimensional State Space

In Section II-B, we discussed the computational and modeling challenges associated with using separate GPs for each dimension of the transition function in high-dimensional state spaces. To address these issues, we propose to warp a single shared GP using normalizing flows [45], [40] to fit each dimension of the transition function, that is,

$$\tilde{f}(\cdot) \sim \mathcal{GP}(0, k(\cdot, \cdot)), \quad \mathbf{f}_d(\cdot) = \mathbb{G}_{\theta_d}(\tilde{f}(\cdot)), \quad d=1, \dots, d_x, \quad (6)$$

where each dimension-specific normalizing flow,  $\mathbb{G}_{\theta_d}(\cdot)$ , is an element-wise, invertible and differentiable (bijective) function parameterized by  $\theta_d \in \Theta$ . Two specific examples are provided below.

**Example 1.** If  $\mathbb{G}_{\theta_d}(\cdot)$  is a simple linear flow, then we have

$$\mathbf{f}_d(\cdot) = \alpha_d \cdot \tilde{f}(\cdot) + \beta_d,$$

with  $\theta_d = [\alpha_d, \beta_d]^\top \in \mathbb{R}^2$ .

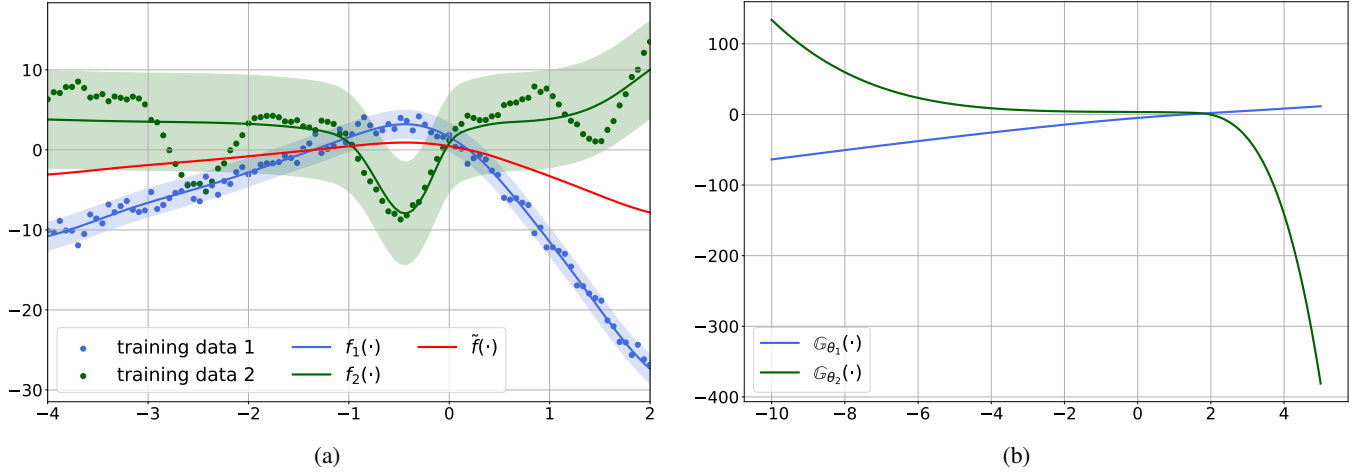


Fig. 2: Illustration of the limited flexibility of the warped GPs as presented in Eq. (6). (a) Two warped GPs: one (—) effectively captures data pattern, while the other (—) falls short. (b) Associated normalizing flows that coordinate-wisely transform the shared GP (—), where the x-axis represents  $\tilde{f}(\mathbf{x})$ , and y-axis is  $\mathbb{G}_{\theta}(\tilde{f}(\mathbf{x}))$ .

**Example 2.** If  $\mathbb{G}_{\theta_d}(\cdot)$  is a Sinh-Arcsinh-Linear (SAL) flow [47], [48], we have:

$$\mathbf{f}_d(\cdot) = \alpha_d \sinh \left[ \varphi_d \operatorname{arcsinh} \left( \tilde{f}(\cdot) \right) - \gamma_d \right] + \beta_d,$$

with  $\boldsymbol{\theta}_d = [\alpha_d, \beta_d, \gamma_d, \varphi_d]^\top \in \mathbb{R}^4$ .

More complex flows can be achieved by stacking additional layers of SAL flow and/or incorporating more advanced deep neural network-based flows, such as RealNVP [49].

The primary advantage of this methodology lies in its elimination of multiple independent GPs, thereby enabling circumvent the  $\mathcal{O}(d_x m^3)$  computational complexity and quadratic parameter proliferation mentioned in Section II-B3. Furthermore, the warped GPs are dependent which can address the key limitation of independence modeling in the conventional GPSSM works.

However, the warped GPs remain stationary random processes and may still lack the flexibility required to capture complex latent state patterns, leading to suboptimal learning performance [40]. An intuitive illustrative example is shown in Fig. 2a, where the learned element-wise flow  $\mathbb{G}_{\theta_1}$  warps  $\tilde{f}$  to obtain  $\mathbf{f}_1$ , effectively fitting simpler data patterns due to its near-linear behavior (see Fig. 2b). However, when faced with more complex, non-stationary data trajectories, the warped GP struggles to capture these patterns. As demonstrated by the example of  $\mathbf{f}_2$ , it fails to adequately model intricate local variations, resulting in large modeling uncertainty. This example highlights the limited capacity of the warped GP in Eq. (6), particularly when modeling complex, non-stationary transition functions in dynamic systems.

To enhance the modeling flexibility, we draw inspiration from recent advancements [50], [51] and introduce non-stationarity and input dependence into the warped GPs. Specifically, we generate non-stationary processes  $\{\mathbf{f}_d(\cdot)\}_{d=1}^{d_x}$  by making the flow parameters depend on the input through a shallow neural network, denoted as  $\text{NN} : \mathcal{X} \mapsto \Theta$ , and parameterized by a weight vector  $\mathbf{w}$ . Formally, in the context

of SSM, this is expressed as<sup>1</sup>:

$$\boldsymbol{\theta}_t = \text{NN}_{\mathbf{w}}(\mathbf{x}_{t-1}), \quad (7)$$

where  $\boldsymbol{\theta}_t = \{\theta_{t,d}\}_{d=1}^{d_x}$ . In this case, the flow parameters vary with the input at each time step  $t$ , enabling the capture of local variation patterns and facilitating the modeling of time-varying transition functions. Additionally, note that the efficient parameter amortization learning shown in Eq. (7) can avoid the issue of the number of flow parameters linearly increasing with time step  $t$ . We may further impose a prior  $p_{\psi}(\mathbf{w})$  over  $\mathbf{w}$  (e.g.,  $\mathbf{w} \sim \mathcal{N}(\mathbf{w}|\mathbf{0}, \mathbf{I})$ ) with hyperparameter  $\psi$ , thereby regularizing the neural network's parameters and mitigating overfitting issues.

In summary, our modeling approach can be mathematically expressed as follows:

$$\tilde{f}(\cdot) \sim \mathcal{GP}(0, k(\cdot, \cdot)), \quad \mathbf{w} \sim p_{\psi}(\mathbf{w}), \quad (8a)$$

$$\boldsymbol{\theta}_t = \text{NN}_{\mathbf{w}}(\mathbf{x}_{t-1}), \quad \mathbf{f}_d(\cdot) = \mathbb{G}_{\theta_{t,d}}(\tilde{f}(\cdot)), \quad d=1, \dots, d_x, \quad (8b)$$

where  $\{\mathbf{f}_d(\cdot)\}_{d=1}^{d_x}$  implicitly characterize  $d_x$  random processes [44]. To better understand the modeling, Fig. 3 illustrates the corresponding graphical representation with  $p_{\psi}(\mathbf{w}) = \delta(\mathbf{w} - \bar{\mathbf{w}})$ , where  $\delta(\cdot)$  is the Dirac delta function and  $\bar{\mathbf{w}}$  is a deterministic vector, and the following example extends the Example 1 provides a more concrete illustration.

**Example 3.** In the case of the linear flow, we have

$$\mathbf{f}(\cdot) = \boldsymbol{\alpha}_t \cdot \tilde{f}(\cdot) + \boldsymbol{\beta}_t, \quad (9a)$$

$$\boldsymbol{\theta}_t = \text{NN}_{\mathbf{w}}(\mathbf{x}_{t-1}), \quad \mathbf{w} \sim p_{\psi}(\mathbf{w}). \quad (9b)$$

where  $\boldsymbol{\theta}_t = [\boldsymbol{\alpha}_t^\top, \boldsymbol{\beta}_t^\top]^\top$ , and  $\boldsymbol{\alpha}_t = \{\alpha_{t,d}\}_{d=1}^{d_x}$ ,  $\boldsymbol{\beta}_t = \{\beta_{t,d}\}_{d=1}^{d_x}$ .

It is noteworthy that this modeling approach, also known as the efficient transformed Gaussian process (ETGP) in the GP

<sup>1</sup>Note that  $\mathbf{x}_t$  can always be extended to accommodate control systems incorporating a deterministic control input  $\mathbf{c}_t \in \mathbb{R}^{d_c}$  by augmenting the latent state to  $[\mathbf{x}_t^\top, \mathbf{c}_t^\top]^\top \in \mathbb{R}^{d_x+d_c}$ . For brevity, however, we omit explicit reference to  $\mathbf{c}_t$  in our notation throughout this paper.

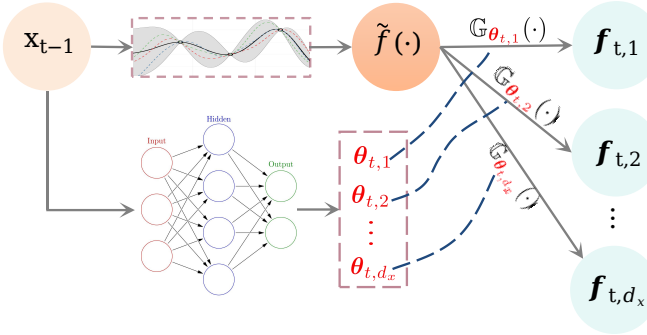


Fig. 3: ETGP transition function in SSMs

literature, was initially proposed to address large-scale multi-class classification problems [50]. The efficiency stems from the use of a single GP and the constant scaling of GP operations with respect to the number of classes, which significantly speeds up computations. In this work, we adapt it to model the high-dimensional transition function in SSMs. Additionally, ETGP implicitly characterizes  $d_x$  dependent random processes [44], a dependence that has been overlooked in prior GPSSM literature. A more detailed insight is provided below.

**Corollary 1.** *If  $p_\psi(\mathbf{w}) = \delta(\mathbf{w} - \bar{\mathbf{w}})$ , where  $\bar{\mathbf{w}}$  is a deterministic vector, then the ETGP defined in Example 3 becomes a  $d_x$ -dimensional dependent non-stationary Gaussian process with time-dependent covariance. Specifically, at arbitrary time steps  $t$  and  $t'$ , we have*

$$\begin{bmatrix} \mathbf{f}(\mathbf{x}_{t-1}) \\ \mathbf{f}(\mathbf{x}_{t'-1}) \end{bmatrix} \sim \mathcal{N}\left(\begin{bmatrix} \boldsymbol{\beta}_t \\ \boldsymbol{\beta}_{t'} \end{bmatrix}, \boldsymbol{\Lambda}_{t,t'}\right), \quad (10)$$

where the covariance matrix  $\boldsymbol{\Lambda}_{t,t'} \in \mathbb{R}^{2d_x \times 2d_x}$  is given by

$$\boldsymbol{\Lambda}_{t,t'} = \begin{bmatrix} k(\mathbf{x}_{t-1}, \mathbf{x}_{t-1}) \cdot \boldsymbol{\alpha}_t \boldsymbol{\alpha}_t^\top & k(\mathbf{x}_{t-1}, \mathbf{x}_{t'-1}) \cdot \boldsymbol{\alpha}_t \boldsymbol{\alpha}_{t'}^\top \\ k(\mathbf{x}_{t'-1}, \mathbf{x}_{t-1}) \cdot \boldsymbol{\alpha}_{t'} \boldsymbol{\alpha}_t^\top & k(\mathbf{x}_{t'-1}, \mathbf{x}_{t'-1}) \cdot \boldsymbol{\alpha}_{t'} \boldsymbol{\alpha}_{t'}^\top \end{bmatrix}. \quad (11)$$

*Proof.* This result follows straightforwardly from the Gaussianity and the linearity property of covariance, which can be found in Appendix A.  $\square$

With the efficient and flexible function prior defined by ETGP  $\mathbf{f}(\cdot) = \{\mathbf{f}_d(\cdot)\}_{d=1}^{d_x}$ , we now can define our proposed SSM, termed ETGPSSM, compactly expressed as follows:

$$\mathbf{f}(\cdot) \sim \mathcal{ETGP}(\tilde{\mathbf{f}}(\cdot), p_\psi(\mathbf{w})), \quad (12a)$$

$$\mathbf{x}_0 \sim p(\mathbf{x}_0), \quad (12b)$$

$$\mathbf{f}_t = \mathbf{f}(\mathbf{x}_{t-1}), \quad (12c)$$

$$\mathbf{x}_t | \mathbf{f}_t \sim \mathcal{N}(\mathbf{x}_t | \mathbf{f}_t, \mathbf{Q}), \quad (12d)$$

$$\mathbf{y}_t | \mathbf{x}_t \sim \mathcal{N}(\mathbf{y}_t | \mathbf{C}\mathbf{x}_t, \mathbf{R}), \quad (12e)$$

where the ETGP prior is characterized by the associated GP  $\tilde{\mathbf{f}}(\cdot)$ , neural network weight prior  $p_\psi(\mathbf{w})$ , and the normalizing flows, see Eq. (8). In this paper, unless otherwise specified, we focus on the linear flow shown in Example 3 for simplicity and illustrative purposes. Additionally, the linear flow requires learning only 2 parameters per dimension, making it more efficient compared to other types of normalizing flows. We also

assume that the prior distribution of the initial state,  $p(\mathbf{x}_0)$ , is Gaussian and known for simplicity.

**Remark 1.** *In contrast to existing GPSSMs, the  $\{\mathbf{f}_d(\cdot)\}_{d=1}^{d_x}$  in the ETGPSSM are dependent, as they are both transformed random processes derived from a shared GP and common weight priors (see Corollary 1). Furthermore, as these induced random processes are non-stationary (see Corollary 1), they are well-suited for modeling time-varying transition functions.*

The primary objective in ETGPSSM, as in GPSSM, is the joint estimation of model hyperparameters  $\boldsymbol{\vartheta} = \{\boldsymbol{\theta}_{gp}, \boldsymbol{\psi}, \mathbf{Q}, \mathbf{R}\}$  and inference of both the ETGP and latent states. More specifically, given a sequence of observations  $\bar{\mathbf{y}} = \mathbf{y}_{1:T} = \{\mathbf{y}_t\}_{t=1}^T$ , with  $T \in \mathbb{Z}_+$ , the task is to estimate  $\boldsymbol{\vartheta}$  and compute the posterior distributions<sup>2</sup>  $p(\mathbf{f}(\cdot) | \bar{\mathbf{y}})$  for the ETGP and  $p(\bar{\mathbf{x}} | \bar{\mathbf{y}})$  for the latent states, where  $\bar{\mathbf{x}} = \mathbf{x}_{0:T} = \{\mathbf{x}_t\}_{t=0}^T$ .

However, the marginal distribution  $p(\mathbf{y}_{1:T} | \boldsymbol{\vartheta})$  is intractable, complicating hyperparameter estimation via model evidence maximization and rendering posterior distributions intractable. Additionally, unlike the GP, which explicitly defines the forms of the prior and posterior (see Eqs. (2) and (3)), the ETGP is an implicit random process. It lacks explicit forms for the prior<sup>3</sup> and posterior distributions [44], rendering the inference of the ETGP non-trivial.

The next subsection will show how we address these issues to jointly learn the model hyperparameters and perform Bayesian inference of the ETGP and latent states.

## B. Approximate Bayesian Inference

To address the intractability of the marginal distribution  $p(\bar{\mathbf{y}} | \boldsymbol{\vartheta})$ , we resort to variational inference, which involves maximizing an evidence lower bound (ELBO) on the logarithm of the marginal likelihood [52]. The ELBO, denoted as  $\mathcal{L}$ , can be generally constructed as follows:

$$\mathcal{L} = \mathbb{E}_{q(\bar{\mathbf{x}}, \mathbf{f}(\cdot))} \left[ \log \frac{p(\bar{\mathbf{x}}, \mathbf{f}(\cdot), \bar{\mathbf{y}})}{q(\bar{\mathbf{x}}, \mathbf{f}(\cdot))} \right], \quad (13)$$

so that the difference between  $\log p(\bar{\mathbf{y}} | \boldsymbol{\vartheta})$  and  $\mathcal{L}$  equals the Kullback-Leibler (KL) divergence between the introduced variational approximation  $q(\bar{\mathbf{x}}, \mathbf{f}(\cdot))$  and the true posterior  $p(\bar{\mathbf{x}}, \mathbf{f}(\cdot) | \bar{\mathbf{y}})$ . We then can jointly maximize  $\mathcal{L}$  with respect to  $\boldsymbol{\vartheta}$  and the variational distribution  $q(\bar{\mathbf{x}}, \mathbf{f}(\cdot))$  to obtain the model hyperparameter estimates and the approximation of the posterior distribution  $p(\bar{\mathbf{x}}, \mathbf{f}(\cdot) | \bar{\mathbf{y}})$ .

However, as mentioned earlier, the absence of explicit expressions for the ETGP's prior and posterior prevents the expansion of the ELBO in Eq. (13), rendering variational inference challenging. To address this issue, instead of directly dealing with ETGP in function space, we follow the generative process of ETGP as illustrated in Fig. 3 and infer the posterior distributions of  $\tilde{\mathbf{f}}$  and  $\mathbf{w}$ , which collectively represent the ETGP posterior. Specifically, the joint distribution of the ETGPSSM model we consider is expressed as:

$$p(\bar{\mathbf{y}}, \bar{\mathbf{x}}, \mathbf{w}, \tilde{\mathbf{f}}) = p(\bar{\mathbf{y}}, \bar{\mathbf{x}} | \mathbf{w}, \tilde{\mathbf{f}}) p_\psi(\mathbf{w}) p(\tilde{\mathbf{f}}), \quad (14)$$

<sup>2</sup>We denote the ETGP posterior as  $p(\mathbf{f}(\cdot) | \bar{\mathbf{y}})$ , with slight notation abuse.

<sup>3</sup>Marginalizing the GP and  $\mathbf{w}$  to obtain  $p(\mathbf{f}(\cdot))$  is intractable.

where  $p(\tilde{f})$  represents the GP prior with a bit of notation abuse [33] and  $p_{\psi}(\mathbf{w}) = \mathcal{N}(\mathbf{w}|\mathbf{0}, \text{diag}(\psi))$ . The term  $p(\vec{\mathbf{y}}, \vec{\mathbf{x}}|\mathbf{w}, \tilde{f})$  is factorized as:

$$p(\vec{\mathbf{y}}, \vec{\mathbf{x}}|\mathbf{w}, \tilde{f}) = p(\mathbf{x}_0) \prod_{t=1}^T p(\mathbf{y}_t|\mathbf{x}_t)p(\mathbf{x}_t|\mathbf{w}, \tilde{f}, \mathbf{x}_{t-1}), \quad (15)$$

with the transition term specified as:

$$\begin{aligned} p(\mathbf{x}_t|\mathbf{w}, \tilde{f}, \mathbf{x}_{t-1}) &= \int p(\mathbf{x}_t|\mathbf{f}_t)p(\mathbf{f}_t|\mathbf{w}, \tilde{f}, \mathbf{x}_{t-1})d\mathbf{f}_t \\ &= \mathcal{N}\left(\mathbf{x}_t \mid \alpha_t \cdot \tilde{f}(\mathbf{x}_{t-1}) + \beta_t, \mathbf{Q}\right). \end{aligned} \quad (16)$$

To infer the latent variables  $\{\vec{\mathbf{x}}, \mathbf{w}\}$  and GP  $\tilde{f}$ , we adopt the following variational distribution:

$$q(\vec{\mathbf{x}}, \tilde{f}, \mathbf{w}) = q(\tilde{f})q(\mathbf{w})q(\mathbf{x}_0) \prod_{t=1}^T q(\mathbf{x}_t|\mathbf{w}, \tilde{f}, \mathbf{x}_{t-1}). \quad (17)$$

Here the variational distributions of  $\mathbf{x}_0$  and  $\mathbf{w}$  are defined as follows:

$$\begin{cases} q(\mathbf{x}_0) = \mathcal{N}(\mathbf{x}_0|\mathbf{m}_0, \mathbf{L}_0\mathbf{L}_0^\top), \\ q(\mathbf{w}) = \mathcal{N}(\mathbf{w}|\mathbf{m}_w, \text{diag}(\sigma_w^2)), \end{cases} \quad (18)$$

where  $\mathbf{m}_0 \in \mathbb{R}^{d_x}$ , lower-triangular matrix  $\mathbf{L}_0 \in \mathbb{R}^{d_x \times d_x}$ , and  $\{\mathbf{w}, \sigma_w^2\}$  are free variational parameters.

For  $q(\tilde{f})$ , we will adopt a sparse GP approximation [42], [43], which is ubiquitous in GP-based latent variable models [53], [54], [12], as it provides analytical as well as computational tractability. The general idea of the sparse GP involves augmenting the corresponding GP by introducing a set of inducing points  $\vec{\mathbf{z}} = \{\mathbf{z}_i\}_{i=1}^M$  and  $\mathbf{u} = \{\mathbf{u}_i\}_{i=1}^M$ ,  $M \ll T$ , that will serve as a surrogate for the GP. Here,  $\mathbf{u} \sim \mathcal{N}(\mathbf{0}, \mathbf{K}_{\vec{\mathbf{z}}, \vec{\mathbf{z}}})$  and  $\mathbf{z}_i \in \mathbb{R}^{d_x} \subset \mathcal{X}$ . Specifically, for the augmented GP prior,

$$p(\tilde{f}, \mathbf{u}) = p(\tilde{f}|\mathbf{u})p(\mathbf{u}), \quad (19)$$

we approximate the corresponding GP posterior by specifying a free Gaussian density on the function values  $\mathbf{u}$  at  $M$  locations,  $q(\mathbf{u}) = \mathcal{N}(\mathbf{u}|\mathbf{m}, \mathbf{S})$ , and using the prior conditional for the rest of the GP, i.e.,

$$q(\tilde{f}, \mathbf{u}) = p(\tilde{f}|\mathbf{u})q(\mathbf{u}). \quad (20)$$

In this way, the approximate GP posterior is

$$q(\tilde{f}) = \int q(\tilde{f}, \mathbf{u})d\mathbf{u} = \mathcal{N}(\tilde{f}(\mathbf{x}_*) \mid \xi_p(\mathbf{x}_*), \Xi_p(\mathbf{x}_*)), \quad (21)$$

where

$$\xi_p(\mathbf{x}_*) = \mathbf{K}_{\mathbf{x}_*, \vec{\mathbf{z}}}\mathbf{K}_{\vec{\mathbf{z}}, \vec{\mathbf{z}}}^{-1}\mathbf{m}, \quad (22)$$

$$\Xi_p(\mathbf{x}_*) = \mathbf{K}_{\mathbf{x}_*, \mathbf{x}_*} - \mathbf{K}_{\mathbf{x}_*, \vec{\mathbf{z}}}\mathbf{K}_{\vec{\mathbf{z}}, \vec{\mathbf{z}}}^{-1}[\mathbf{K}_{\vec{\mathbf{z}}, \vec{\mathbf{z}}} - \mathbf{S}]\mathbf{K}_{\vec{\mathbf{z}}, \vec{\mathbf{z}}}^{-1}\mathbf{K}_{\vec{\mathbf{z}}, \mathbf{x}_*}^\top, \quad (23)$$

resulting in a computational complexity that scales as  $\mathcal{O}(M^3)$  instead of  $\mathcal{O}(T^3)$ .

**Remark 2** (Efficiency). *Compared to existing GPSSMs, the computational complexity of ETGPSSM is reduced from  $\mathcal{O}(d_x M^3)$  to  $\mathcal{O}(M^3)$  due to the use of a single GP. Furthermore, since only a single GP is involved, the variational parameters (e.g., inducing inputs) do not grow quadratically, as discussed in Section II-B3, demonstrating both parameter-*

*ization efficiency and computational efficiency.*

For  $q(\mathbf{x}_t|\mathbf{w}, \tilde{f}, \mathbf{x}_{t-1})$  in Eq. (17), rather than explicitly assuming a parameterized form for its distribution, which would introduce additional optimization burden [33], we adopt the approach from recent work [39] to infer the state using the established EnKF within the variational learning framework. Specifically, without explicitly assuming the variational distribution, we introduce the following approximation:

**Assumption 1.**

$$q(\mathbf{x}_t|\mathbf{w}, \tilde{f}, \mathbf{x}_{t-1}) \approx p(\mathbf{x}_t|\mathbf{w}, \tilde{f}, \mathbf{x}_{t-1}, \mathbf{y}_{1:t}), \quad (24)$$

which posits that the variational distribution of  $\mathbf{x}_t$  can be approximated by the corresponding filtering distribution. Additionally, we assume that the following filtering distribution can be approximated by a one-step backward smoothing distribution, i.e.,

**Assumption 2.**

$$p(\mathbf{x}_{t-1}|\mathbf{w}, \tilde{f}, \mathbf{y}_{1:t-1}) \approx p(\mathbf{x}_{t-1}|\mathbf{w}, \tilde{f}, \mathbf{y}_{1:t}), \quad (25)$$

The two assumptions are reasonable and detailed justification can be found in Appendix B.

With these two assumptions, we can significantly streamline the evaluation of the ELBO, which is summarized in the following proposition.

**Proposition 1.** *Under the two approximations, and all the assumed variational distributions, together with the model joint distribution in Eq. (14), the ELBO can be reformulated as follows:*

$$\begin{aligned} \mathcal{L} \approx & \mathbb{E}_{q(\mathbf{w}, \tilde{f})} \left[ \sum_{t=1}^T \log p(\mathbf{y}_t|\mathbf{y}_{1:t-1}, \mathbf{w}, \tilde{f}) \right] - \text{KL}(q(\mathbf{u})\|p(\mathbf{u})) \\ & - \text{KL}(q(\mathbf{w})\|p(\mathbf{w})) - \text{KL}(q(\mathbf{x}_0)\|p(\mathbf{x}_0)), \end{aligned} \quad (26)$$

where the first term (log-likelihood) can be analytically evaluated using the EnKF (detailed in Section III-C). The three KL divergence terms can also be computed in closed form, due to the Gaussian nature of the prior and variational distributions [52].

*Proof.* The proof can be found in Appendix B.  $\square$

### C. EnKF-aided ELBO Evaluation

We now demonstrate how to evaluate  $p(\mathbf{y}_t|\mathbf{y}_{1:t-1}, \mathbf{w}, \tilde{f})$  in  $\mathcal{L}$  using the EnKF. The general idea is derived from Bayesian filtering and is straightforward. We first notice that

$$p(\mathbf{y}_t|\mathbf{y}_{1:t-1}, \mathbf{w}, \tilde{f}) = \int p(\mathbf{y}_t|\mathbf{x}_t)p(\mathbf{x}_t|\mathbf{w}, \tilde{f}, \mathbf{y}_{1:t-1})d\mathbf{x}_t, \quad (27)$$

where the prediction distribution,  $p(\mathbf{x}_t|\mathbf{w}, \tilde{f}, \mathbf{y}_{1:t-1}) =$

$$\int \underbrace{p(\mathbf{x}_t|\mathbf{w}, \tilde{f}, \mathbf{x}_{t-1})}_{\text{transition}} \underbrace{p(\mathbf{x}_{t-1}|\mathbf{w}, \tilde{f}, \mathbf{y}_{1:t-1})}_{\text{filtering}} d\mathbf{x}_{t-1}. \quad (28)$$

Consequently, we employ the EnKF, a widely used method for handling nonlinearities and high-dimensional state spaces

[55], to obtain the filtering distribution  $p(\mathbf{x}_t | \mathbf{w}, \tilde{f}, \mathbf{y}_{1:t})$  at each time step  $t$ . Further details are provided below.

1) **Prediction:** Given the ensemble of states  $\{\mathbf{x}_{t-1}^{(i)}\}_{i=1}^N$  from the posterior distribution  $p(\mathbf{x}_{t-1} | \mathbf{w}, \tilde{f}, \mathbf{y}_{1:t-1})$  at time  $t-1$ , and conditioning on  $\mathbf{w} \sim q(\mathbf{w})$  and  $f \sim q(f)$ , we utilize the state transition in Eq. (16) to perform the prediction step. This generates  $N$  predicted samples  $\{\bar{\mathbf{x}}_t^{(i)}\}_{i=1}^N$  as follows:

$$\bar{\mathbf{x}}_t^{(i)} \sim \mathcal{N}\left(\mathbf{x}_t \mid \alpha_t \cdot \tilde{f}(\mathbf{x}_{t-1}^{(i)}) + \beta_t, \mathbf{Q}\right), i = 1, 2, \dots, N. \quad (29)$$

Therefore, the prediction distribution in Eq. (28) is approximated as:

$$p(\mathbf{x}_t | \mathbf{w}, \tilde{f}, \mathbf{y}_{1:t-1}) \approx \mathcal{N}(\mathbf{x}_t \mid \bar{\mathbf{m}}_t, \bar{\mathbf{P}}_t), \quad (30)$$

where

$$\bar{\mathbf{m}}_t = \frac{1}{N} \sum_{i=1}^N \bar{\mathbf{x}}_t^{(i)}, \quad (31a)$$

$$\bar{\mathbf{P}}_t = \frac{1}{N-1} \sum_{i=1}^N \left(\bar{\mathbf{x}}_t^{(i)} - \bar{\mathbf{m}}_t\right) \left(\bar{\mathbf{x}}_t^{(i)} - \bar{\mathbf{m}}_t\right)^\top. \quad (31b)$$

2) **Update:** Observations  $\mathbf{y}_t$  are then assimilated into the predictive ensemble to update the state estimate. Specifically, the predictive ensemble is updated using:

$$\text{update: } \mathbf{x}_t^{(i)} = \bar{\mathbf{x}}_t^{(i)} + \mathbf{G}_t(\mathbf{y}_t + \mathbf{e}_t^{(i)} - \mathbf{C}\bar{\mathbf{x}}_t^{(i)}), \quad (32a)$$

$$\text{reparameterization: } \mathbf{e}_t^{(i)} = \mathbf{0} + \mathbf{R}^{\frac{1}{2}}\boldsymbol{\epsilon}, \boldsymbol{\epsilon} \sim \mathcal{N}(\mathbf{0}, \mathbf{I}_{d_y}), \quad (32b)$$

where  $\mathbf{G}_t$  is the Kalman gain matrix given by:

$$\mathbf{G}_t = \bar{\mathbf{P}}_t \mathbf{C}^\top (\mathbf{C} \bar{\mathbf{P}}_t \mathbf{C}^\top + \mathbf{R})^{-1}. \quad (33)$$

Thus we can obtain the set of  $N$  updated samples  $\{\mathbf{x}_t^{(i)}\}_{i=1}^N$  from the filtering distribution at time step  $t$ . These updated samples allow us to recursively compute the samples and prediction distribution for subsequent time steps.

**Remark 3.** *The prediction and update steps are inherently differentiable, as the sampled latent states become differentiable with respect to the state transition function  $f(\cdot)$  and the noise covariances  $\mathbf{Q}$  and  $\mathbf{R}$ . This property allows for an easy gradient-based optimization (see Algorithm 1), facilitating an efficient learning framework for parameter estimation and model tuning [56], [39].*

Based on the outlined prediction and update steps, the likelihood  $p(\mathbf{y}_t | \mathbf{y}_{1:t-1}, \mathbf{w}, \tilde{f})$  in Eq. (27) can now be evaluated. Specifically, at each time step  $t$ , we have:

$$p(\mathbf{y}_t | \mathbf{y}_{1:t-1}, \mathbf{w}, \tilde{f}) \approx \mathcal{N}(\mathbf{y}_t \mid \mathbf{C}\bar{\mathbf{m}}_t, \mathbf{C}\bar{\mathbf{P}}_t\mathbf{C}^\top), \quad (34)$$

due to the Gaussian prediction distribution, see Eq. (30), and the linear emission model, see Eq. (12e).

Now, we can evaluate our variational lower bound,  $\mathcal{L}$ , as defined in Eq. (26). At each step, we first utilize the reparameterization trick (see e.g. Eq. (32b)) to sample from the Gaussian variational distributions  $q(\mathbf{w})$  and  $q(f)$ . This allows us to numerically obtain an unbiased estimate of the expected log-likelihood,  $\mathbb{E}_{q(\mathbf{w}, f)}[\log p(\mathbf{y}_t | \mathbf{y}_{1:t-1}, \mathbf{w}, \tilde{f})]$ . Due

---

### Algorithm 1 EnKF-aided variational ETGPSSM

---

**Input:**  $\boldsymbol{\vartheta} = \{\boldsymbol{\theta}_{gp}, \psi, \mathbf{Q}, \mathbf{R}\}$ ,  $\zeta$ ,  $\mathbf{y}_{1:T}$ ,  $\mathbf{x}_0^{1:N} \sim q(x_0)$

- 1: **while** iterations not terminated **do**
- 2:    $\mathbf{w} \sim q(\mathbf{w})$ ,  $L_\ell = 0$
- 3:   **for**  $t = 1, 2, \dots, T$  **do**
- 4:     Get  $f$  from  $q(f)$  using Eq. (21) with  $\mathbf{x}_* = \mathbf{x}_{t-1}$
- 5:     Get prediction samples using Eq. (29)
- 6:     Get empirical moments  $\bar{\mathbf{m}}_t, \bar{\mathbf{P}}_t$  using Eq. (31)
- 7:     Get Kalman gain:  $\bar{\mathbf{G}}_t = \bar{\mathbf{P}}_t \mathbf{C}^\top (\mathbf{C} \bar{\mathbf{P}}_t \mathbf{C}^\top + \mathbf{R})^{-1}$
- 8:     Get updated samples using Eq. (32)
- 9:     Evaluate the log-likelihood using Eq. (34), and
 
$$L_\ell = L_\ell + \log p(\mathbf{y}_t | \mathbf{y}_{1:t-1}, \mathbf{w}, \tilde{f})$$
- 10:   **end for**
- 11:   Evaluate  $\mathcal{L}$  based on  $L_\ell$  and Eq. (26)
- 12:   Maximize  $\mathcal{L}$  and update  $\boldsymbol{\vartheta}, \zeta$  using Adam [59]
- 13: **end while**

**Output:** EnKF particles  $\{\mathbf{x}_{0:T}^{(i)}\}_{i=1}^N$ , model parameters  $\boldsymbol{\vartheta}$ , and variational parameters  $\zeta$ .

---

to the reparameterization trick [57],  $\mathcal{L}$  is differentiable with respect to the model parameters  $\boldsymbol{\vartheta} = \{\boldsymbol{\theta}_{gp}, \psi, \mathbf{Q}, \mathbf{R}\}$  and the variational parameters  $\zeta = \{\mathbf{m}_0, \mathbf{L}_0, \mathbf{m}_w, \sigma_w^2, \mathbf{m}, \mathbf{S}, \bar{\mathbf{z}}\}$ . Consequently, we leverage modern differentiation tools, such as PyTorch, to automatically compute the gradients through backpropagation through time (BPTT) and apply gradient-based optimization methods (e.g., Adam) to maximize  $\mathcal{L}$  [58], [59]. The detailed routine for implementing our EnKF-aided ETGPSSM is summarized in Algorithm 1. In the next section, we empirically evaluate the performance of ETGPSSM across various datasets.

## IV. EXPERIMENTS

We first demonstrate the advantages of ETGPSSM in learning non-stationary dynamical systems in Section IV-A. Next, in Section IV-B, we highlight the computational efficiency and filtering performance of ETGPSSM in chaotic high-dimensional dynamical systems. Finally, Section IV-C showcases the superior prediction performance of ETGPSSM using multiple real-world time series datasets. More experimental details can be found in the accompanying source code, which is publicly available online.<sup>4</sup>

### A. Non-Stationary Dynamical System Learning

This subsection demonstrates the superior modeling capabilities of ETGPSSM over existing GPSSM and neural network-based methods by evaluating the learning performance on the following underlying dynamical system:

$$\mathbf{x}_{t+1} = f(\mathbf{x}_t) + \mathbf{v}_t, \quad \mathbf{v}_t \sim \mathcal{N}(0, \sigma_Q^2), \quad (35a)$$

$$\mathbf{y}_t = \mathbf{x}_t + \mathbf{e}_t, \quad \mathbf{e}_t \sim \mathcal{N}(0, \sigma_R^2), \quad (35b)$$

<sup>4</sup>[https://github.com/zhidilin/gpssmProj/tree/main/high\\_dim\\_GPSSM](https://github.com/zhidilin/gpssmProj/tree/main/high_dim_GPSSM)

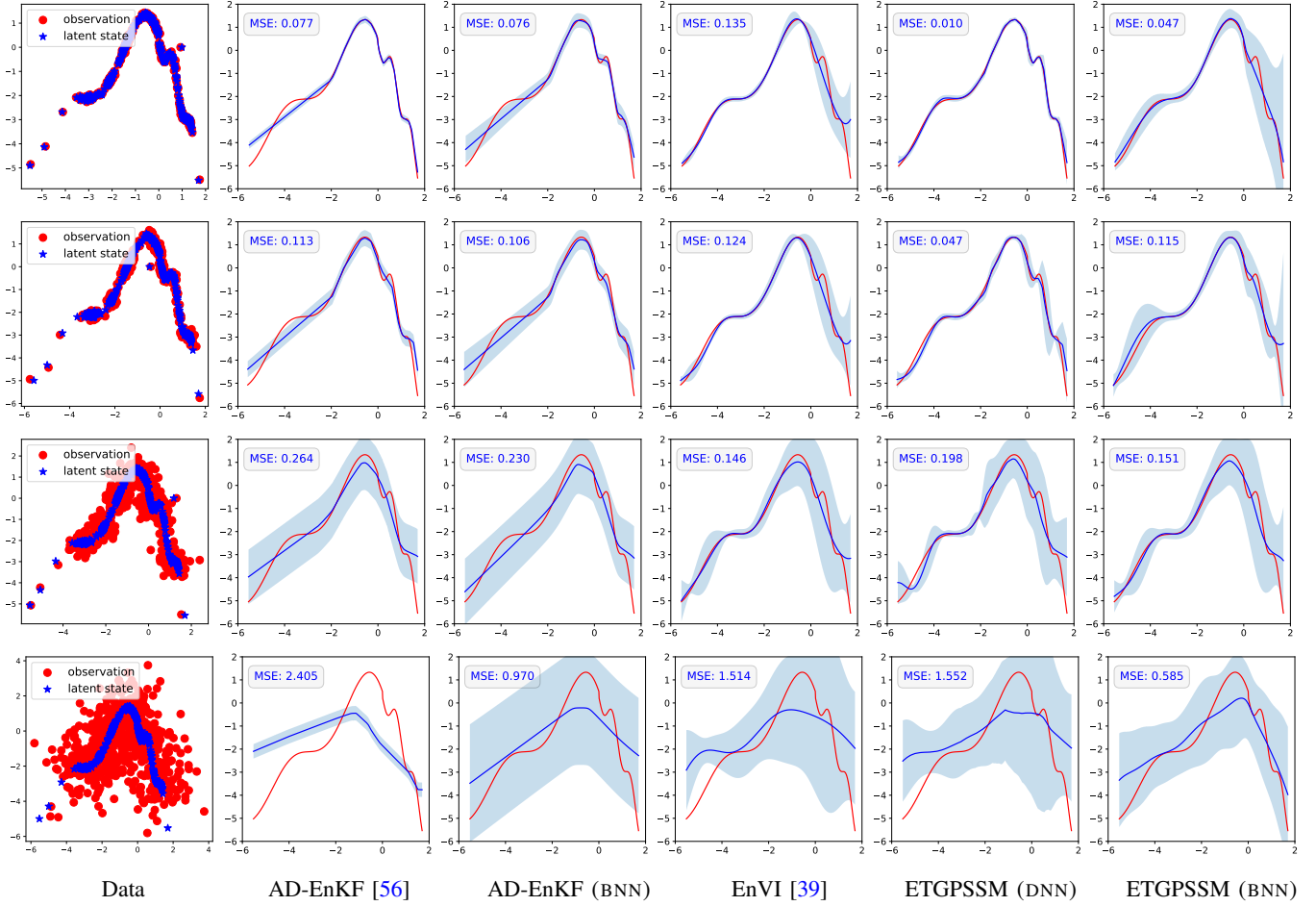


Fig. 4: Non-stationary *kink* transition function learning performance (mean  $\pm 2\sigma$ ) using various methods across different levels of emission noise ( $\sigma_R^2 \in \{0.0008, 0.008, 0.08, 0.8\}$ , from top to bottom). The blue curve ( $\text{—}$ ) represents the learned mean function, while the red line ( $\text{—}$ ) indicates the true system transition function. The shaded blue region depicts the confidence interval.

where the *non-stationary kink function*  $f(\mathbf{x})$  is defined as:

$$f(\mathbf{x}) = \underbrace{\left[ 0.8 + (\mathbf{x} + 0.2) \left( 1 - \frac{5}{1 + \exp(-2\mathbf{x})} \right) \right]}_{\text{“kink” function}} s(\mathbf{x}) - o(\mathbf{x}) \quad (36)$$

with a slope function:

$$s(\mathbf{x}) = \begin{cases} 1 - 0.5 \exp(-0.5\mathbf{x}), & \mathbf{x} > 0, \\ 1, & \mathbf{x} \leq 0, \end{cases} \quad (37)$$

and an oscillatory function:

$$o(\mathbf{x}) = \begin{cases} 0.5 \sin(8\mathbf{x}), & \mathbf{x} > 0, \\ 0.5 \sin(2\mathbf{x}), & \mathbf{x} \leq 0. \end{cases} \quad (38)$$

The slope and oscillatory functions create non-stationary pattern across different regions of the “kink” function (see Fig. 4).

Using this underlying SSM, we generate training data  $\mathbf{y}_{1:T}$  by fixing  $\sigma_Q^2$  at 0.05 and varying  $\sigma_R^2$  systematically across the set  $\{0.0008, 0.008, 0.08, 0.8\}$ , resulting in four sets of  $T = 600$  observations each for training purposes. To demonstrate the advantages of ETGPSSM, we compare it

with state-of-the-art (SOTA) neural network-based AD-EnKFs [56] and GP-based EnVI [39]. Consistent with previous works [33], [39], we retain the true emission model and allow the transition model to be learned in all methods, ensuring a fair comparison within the latent space. The system dynamics learning results across different methods are shown in Fig. 4, where our method is represented in the last two columns. The suffixes “DNN” and “BNN” in brackets indicate the network types—Bayesian neural network (BNN) or deep neural network (DNN)—used in our model (see Fig. 3).

The results in Fig. 4 demonstrate that ETGPSSMs consistently achieve superior system dynamics learning performance. Under small observational noise levels ( $\sigma_R^2 = \{0.0008, 0.008\}$ ), ETGPSSMs—particularly ETGPSSM with DNN—excel in learning the dynamics of non-stationary systems. This advantage arises from their ability to combine the strengths of neural networks for modeling non-stationary functions and GPs for stationary functions. In contrast, their competitor, AD-EnKFs, fails to capture the smooth left segment of the kink function and performs well only on the more zigzag right segment. Meanwhile, EnVI, the SOTA GPSSM,

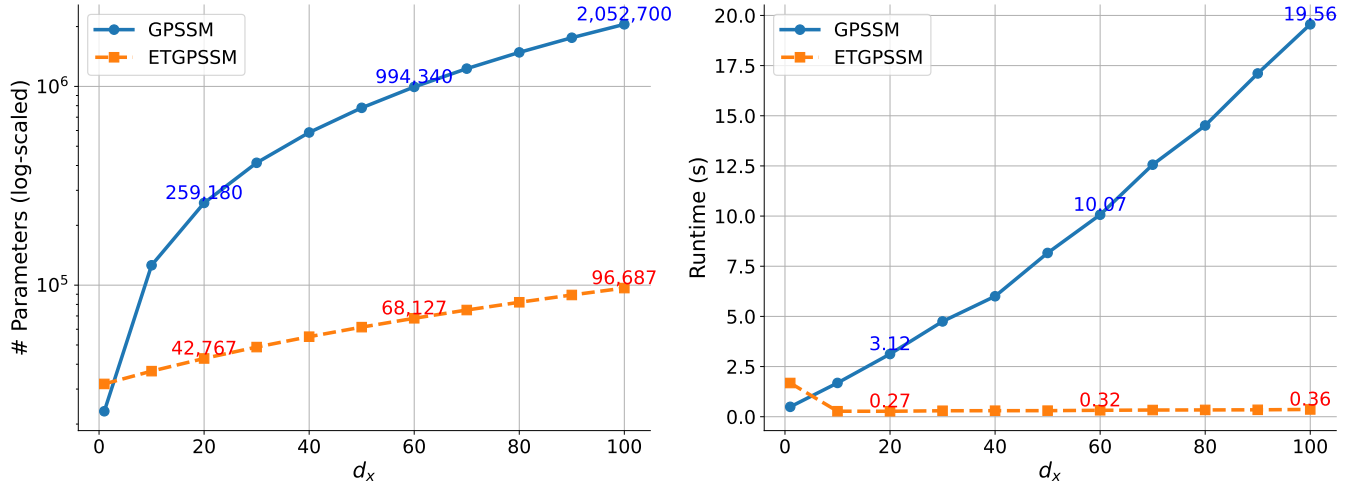


Fig. 5: **(Left)** The number of parameters in ETGPSSM grows linearly with the state dimension  $d_x$ , whereas in GPSSM, it scales quadratically. **(Right)** ETGPSSM maintains low computational costs as  $d_x$  increases, while GPSSM exhibits linear growth.

struggles to model the non-stationary characteristics of the kink function and fails to capture the zigzag segment.

When observational noise interference becomes more significant ( $\sigma_R^2 = \{0.08, 0.8\}$ ), the learning performance of all methods deteriorates. This is due to the higher estimation errors in the latent states, which hinder precise system dynamics learning. Nevertheless, ETGPSSMs continue to demonstrate strong learning performance. Notably, in this scenario, BNN-based methods, particularly ETGPSSM (BNN), exhibit superior performance and more reliable uncertainty quantification compared to their DNN-based counterparts. This highlights the advantage of the inherent regularization of Bayesian methods, which provides learning robustness in the presence of significant observational noise.

### B. High-Dimensional Latent State Estimation

In this subsection, we focus on latent state estimation in the Lorenz-96 system, a mathematical model for studying chaotic behavior in weather and climate dynamics [60]. The system consists of  $d_x \in \mathbb{Z}_+$  coupled ordinary differential equations (ODEs):

$$\frac{d\mathbf{x}_{t,d}}{dt} = (\mathbf{x}_{t,d+1} - \mathbf{x}_{t,d-2})\mathbf{x}_{t,d-1} - \mathbf{x}_{t,d} + F, \quad 1 \leq d \leq d_x.$$

Here the constant forcing parameter  $F$  is set to 8, resulting in a fully chaotic dynamic [60], where small variations in initial conditions lead to vastly different trajectories. The dynamics model is discretized using the Euler method, and at each time step  $t$ , observations are generated through a linear emission model ( $\mathbf{C} = \mathbf{I}$ ) with Gaussian additive noise, where the noise covariance is given by  $\mathbf{R} = 4.0\mathbf{I}$ .

We first empirically demonstrate the efficiency advantage of ETGPSSM in high-dimensional latent state spaces, as depicted in Fig. 5. The figure illustrates the computational efficiency and parameter scalability of ETGPSSM compared to traditional GPSSM across varying latent state dimensions. As shown in the left panel, the number of parameters in ETGPSSM grows linearly with the state dimension, whereas

GPSSM exhibits a quadratic growth in parameters. This linear scaling in ETGPSSM is achieved by leveraging a single shared GP and normalizing flows, which significantly reduces the parameter count compared to the independent GPs used in GPSSM.

The right panel of Fig. 5 illustrates the computational efficiency of ETGPSSM by comparing the one-sample execution time for transition evaluation (i.e., Eq. (1a)). Notably, ETGPSSM maintains consistently low running times across increasing state dimensions, whereas GPSSM exhibits rapid growth in computational cost. For instance, at  $d_x = 100$ , ETGPSSM completes the evaluation in 0.36 seconds, significantly outperforming GPSSM, which requires 19.56 seconds. This efficiency stems from the reduced computational complexity of ETGPSSM, which scales as  $\mathcal{O}(M^3)$  due to its use of a single GP, in contrast to GPSSM's  $\mathcal{O}(d_x M^3)$  complexity. These results demonstrate that ETGPSSM not only scales more efficiently with increasing state dimensions but also maintains computational tractability in high-dimensional settings, making it a practical choice for modeling complex, chaotic systems like the Lorenz-96 system.

We next fix the dimension  $d_x = 100$  in the Lorenz-96 system and generate observations of length  $T = 600$  for training ETGPSSM and its competitor, AD-EnKF [56]. The EnVI [39], which already caused out-of-memory errors<sup>5</sup> at  $d_x = 30$  with an ensemble size  $N = 150$ , is excluded due to its prohibitive computational cost in this high-dimensional setting. The corresponding state inference performance after training is shown in Fig. 6, where the performance of EnKF is also included for comparison.

As illustrated in Fig. 6, ETGPSSM achieves a root mean square error (RMSE) of 1.2028, outperforming AD-EnKF, which yields an RMSE of 1.6187. This result highlights the superior filtering performance of ETGPSSM in high-

<sup>5</sup>All experiments were conducted on a machine equipped with an Intel Xeon W7-3545 v6 processor (24 cores, 2.7 GHz), 128 GB of DDR5 RAM, and an NVIDIA RTX 4500 Ada GPU (24 GB VRAM), running Ubuntu 20.04 LTS.

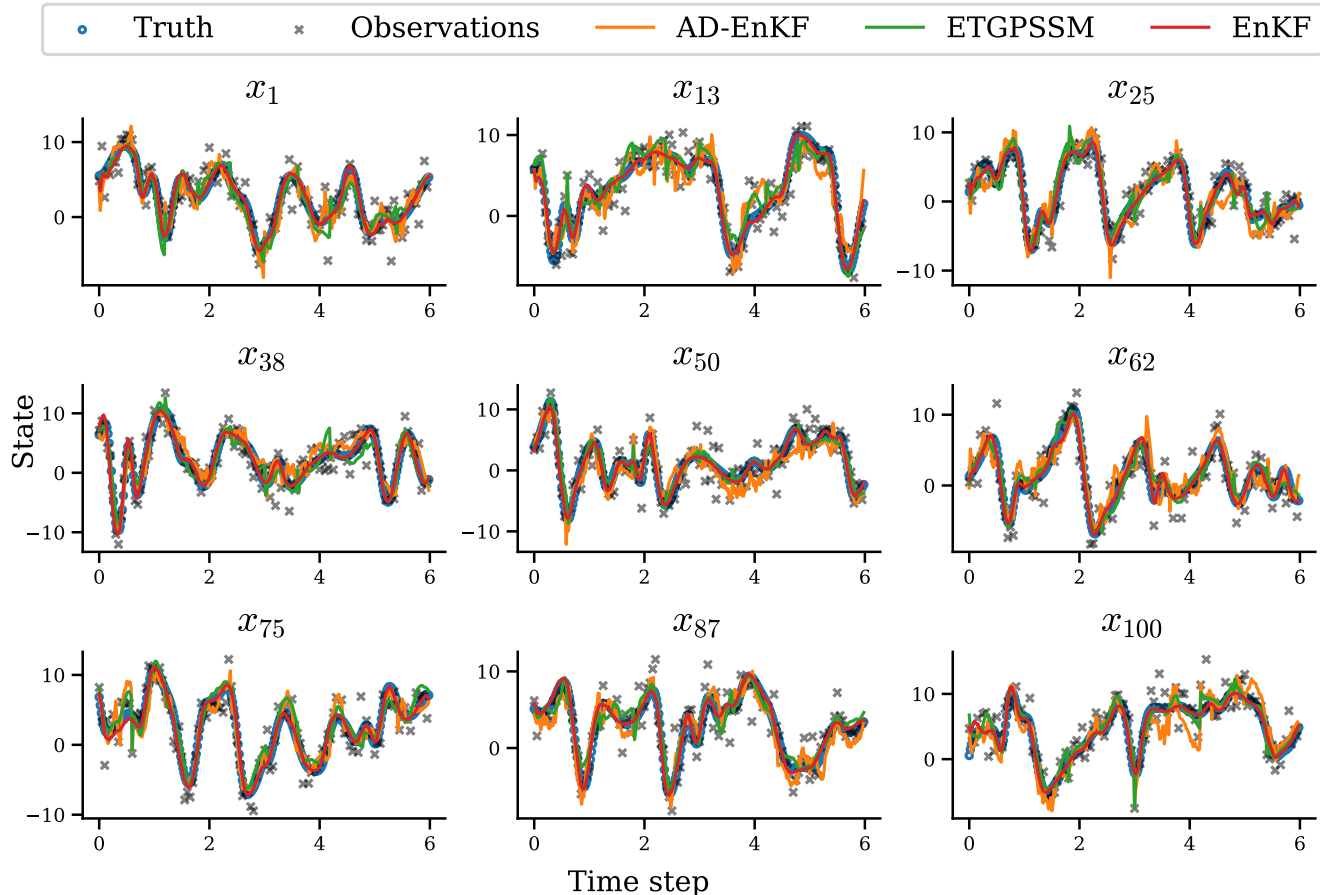


Fig. 6: Latent state estimation performance for 100-dimensional Lorenz-96 system, with 9 dimensions uniformly sampled for visualization. Root mean square error (RMSE) values for different methods: 0.5468 for EnKF, 1.2028 for ETGPSSM, 1.6187 for AD-EnKF, and 1.9855 for the observations.

dimensional chaotic systems. Additionally, the RMSE of the observations (1.9855) serves as a baseline, demonstrating that ETGPSSM significantly reduces the estimation error compared to the raw observations. While EnKF achieves a lower RMSE of 0.5468, it is a well-established filtering method that does not involve learning system dynamics. In contrast, ETGPSSM simultaneously learns the dynamics and performs state inference, making it a more versatile and powerful approach for complex systems.

### C. Real-World Time Series Prediction

In this subsection, we evaluate the prediction performance of ETGPSSM on several real-world time series datasets commonly used for system identification (see Table I). The prediction RMSE results are summarized in Table I, comparing ETGPSSM against SOTA methods, including neural network-based approaches—DKF [8] and AD-EnKF [56]—as well as various GPSSMs: vGPSSM [31], CO-GPSSM [38], PRSSM [32], ODGPSSM [41], VCDT [33], and EnVI [39]. Following previous works, the latent space dimension is set to  $d_x = 4$  for all the methods.

As shown in Table I, ETGPSSM demonstrates competitive performance across all datasets. Notably, on the ACTUATOR

dataset, ETGPSSM (DNN) and ETGPSSM (BNN) both achieve an RMSE of 0.646, outperforming EnVI (0.657) and significantly improving upon AD-EnKFs, which record an RMSE of 0.705. Similarly, on the BALL BEAM and GAS FURNACE datasets, ETGPSSMs attain the first and second lowest RMSEs, highlighting their ability to effectively model system dynamics. However, on datasets such as DRIVE and DRYER, other GPSSMs like PRSSM and EnVI achieve slightly superior performance, with RMSE values of 0.647 and 0.125, respectively. This can be attributed to the relatively low latent state dimension ( $d_x = 4$ ), where traditional GPSSMs, such as PRSSM, ODGPSSM and EnVI, remain highly competitive due to their simpler structure, as discussed in [39]. Nonetheless, we emphasize that our proposed ETGPSSM remains highly competitive even in low-dimensional settings while significantly reducing computational complexity and parameter overhead, ensuring both scalability and efficiency in high-dimensional cases.

In comparison to neural network-based methods like AD-EnKF, the superior performance of ETGPSSM is driven by its ability to integrate the strengths of GPs and neural networks. This hybrid approach allows ETGPSSM to effectively model complex, non-stationary system dynamics while providing

TABLE I: Prediction performance (RMSE) of the different models on the system identification datasets. Mean and standard deviation of the prediction results are shown across ten seeds. The three lowest RMSE values are highlighted in shades of green, with deeper shades indicating lower RMSEs.

Method	ACTUATOR	BALL BEAM	DRIVE	DRYER	GAS FURNACE
<b>DKF [8]</b>	1.204 ± 0.250	0.144 ± 0.005	0.735 ± 0.001	1.465 ± 0.087	5.589 ± 0.066
<b>AD-EnKF [56]</b>	0.705 ± 0.117	0.057 ± 0.006	0.756 ± 0.114	0.182 ± 0.053	1.408 ± 0.090
<b>AD-EnKF (BNN)</b>	0.705 ± 0.088	0.053 ± 0.007	0.896 ± 0.088	0.155 ± 0.030	1.361 ± 0.061
<b>vGPSSM [31]</b>	1.640 ± 0.011	0.268 ± 0.414	0.740 ± 0.010	0.822 ± 0.002	3.676 ± 0.145
<b>CO-GPSSM [38]</b>	0.803 ± 0.011	0.079 ± 0.018	0.736 ± 0.007	0.366 ± 0.146	1.898 ± 0.157
<b>PRSSM [32]</b>	0.691 ± 0.148	0.074 ± 0.010	0.647 ± 0.057	0.174 ± 0.013	1.503 ± 0.196
<b>ODGPSSM [41]</b>	0.666 ± 0.074	0.068 ± 0.006	0.708 ± 0.052	0.171 ± 0.011	1.704 ± 0.560
<b>VCDT [33]</b>	0.815 ± 0.012	0.065 ± 0.005	0.735 ± 0.005	0.667 ± 0.266	2.052 ± 0.163
<b>EnVI [39]</b>	0.657 ± 0.095	0.055 ± 0.002	0.703 ± 0.050	0.125 ± 0.017	1.388 ± 0.123
<b>ETGPSSM (DNN)</b>	0.646 ± 0.081	0.050 ± 0.003	0.668 ± 0.092	0.137 ± 0.030	1.300 ± 0.052
<b>ETGPSSM (BNN)</b>	0.646 ± 0.095	0.053 ± 0.002	0.703 ± 0.028	0.154 ± 0.026	1.313 ± 0.048

reliable and robust predictions—an area where purely neural network-based methods often struggle. This is evident from the results, where neural network-based methods exhibit higher prediction errors. Notably, AD-EnKF (BNN) generally outperforms other network-based approaches, highlighting the benefits of Bayesian treatments, particularly their inherent regularization, which helps mitigate overfitting and improve generalization. In summary, the experimental results demonstrate that ETGPSSM is a powerful and versatile tool for real-world time series prediction.

## V. CONCLUSIONS

In this paper, we introduced ETGPSSM, an efficient and scalable Gaussian process state-space model for high-dimensional, non-stationary dynamical systems. Our approach leverages a transformed GP with normalizing flows and neural networks to enhance modeling flexibility while maintaining computational efficiency. Instead of working in the function space of the implicit process in transformed GPs, we follow their generative process and develop an approximate variational inference algorithm integrated with an EnKF, significantly improving scalability and robustness in learning and inference. Extensive experiments demonstrate that ETGPSSM outperforms existing GPSSMs and neural network-based approaches in accuracy, state estimation, and computational efficiency, highlighting its potential for applications in signal processing, control systems, and time-series analysis.

## APPENDIX A PROOF OF COROLLARY 1

*Proof.* Consider two arbitrary time steps  $t$  and  $t'$ , we have

$$\begin{aligned} \mathbf{f}(\mathbf{x}_{t-1}) &= \boldsymbol{\alpha}_t \cdot \tilde{\mathbf{f}}(\mathbf{x}_{t-1}) + \boldsymbol{\beta}_t, \\ \mathbf{f}(\mathbf{x}_{t'-1}) &= \boldsymbol{\alpha}_{t'} \cdot \tilde{\mathbf{f}}(\mathbf{x}_{t'-1}) + \boldsymbol{\beta}_{t'}. \end{aligned}$$

Since  $\boldsymbol{\theta}_t$  and  $\boldsymbol{\theta}_{t'}$  are deterministic, the joint distribution of  $\mathbf{f}(\mathbf{x}_{t-1})$  and  $\mathbf{f}(\mathbf{x}_{t'-1})$  is Gaussian with mean  $[\boldsymbol{\beta}_t^\top, \boldsymbol{\beta}_{t'}^\top]^\top$ .

The covariance between  $\mathbf{f}(\mathbf{x}_{t-1})$  and  $\mathbf{f}(\mathbf{x}_{t'-1})$  is:

$$\begin{aligned} \boldsymbol{\Lambda}_{t,t'} &= \boldsymbol{\alpha}_t \cdot \text{Cov}(\tilde{\mathbf{f}}(\mathbf{x}_{t-1}), \tilde{\mathbf{f}}(\mathbf{x}_{t'-1})) \cdot \boldsymbol{\alpha}_{t'}^\top \\ &= k(\mathbf{x}_{t-1}, \mathbf{x}_{t'-1}) \cdot \boldsymbol{\alpha}_t \boldsymbol{\alpha}_{t'}^\top. \end{aligned}$$

Similarly, the covariance of  $\mathbf{f}(\mathbf{x}_{t-1})$  with itself is:

$$\text{Cov}(\mathbf{f}(\mathbf{x}_{t-1}), \mathbf{f}(\mathbf{x}_{t-1})) = k(\mathbf{x}_{t-1}, \mathbf{x}_{t-1}) \cdot \boldsymbol{\alpha}_t \boldsymbol{\alpha}_t^\top.$$

The same logic applies to  $\mathbf{f}(\mathbf{x}_{t'-1})$ . Therefore, the covariance matrix  $\boldsymbol{\Lambda}_{t,t'}$  is:

$$\boldsymbol{\Lambda}_{t,t'} = \begin{bmatrix} k(\mathbf{x}_{t-1}, \mathbf{x}_{t-1}) \cdot \boldsymbol{\alpha}_t \boldsymbol{\alpha}_t^\top & k(\mathbf{x}_{t-1}, \mathbf{x}_{t'-1}) \cdot \boldsymbol{\alpha}_t \boldsymbol{\alpha}_{t'}^\top \\ k(\mathbf{x}_{t'-1}, \mathbf{x}_{t-1}) \cdot \boldsymbol{\alpha}_{t'} \boldsymbol{\alpha}_t^\top & k(\mathbf{x}_{t'-1}, \mathbf{x}_{t'-1}) \cdot \boldsymbol{\alpha}_{t'} \boldsymbol{\alpha}_{t'}^\top \end{bmatrix}.$$

□

## APPENDIX B ELBO DERIVATIONS AND APPROXIMATIONS

Given the model joint distribution in Eq. (14) and the variational distribution in Eq. (17), augmented by the sparse GP, we can formulate the ELBO according to the general definition provided in Eq. (13). The detailed derivations are presented in Eq. (39).

From Eq. (39d) to Eq. (39e), we have made the following two assumptions, similar to the work in [39]:

- 1)  $p(\mathbf{x}_{t-1} | \mathbf{w}, \tilde{\mathbf{f}}, \mathbf{y}_{1:t-1}) \approx p(\mathbf{x}_{t-1} | \mathbf{w}, \tilde{\mathbf{f}}, \mathbf{y}_{1:t})$ ,
- 2)  $q(\mathbf{x}_t | \mathbf{w}, \tilde{\mathbf{f}}, \mathbf{x}_{t-1}) \approx p(\mathbf{x}_t | \mathbf{w}, \tilde{\mathbf{f}}, \mathbf{x}_{t-1}, \mathbf{y}_{1:t})$ .

The transition from Eq. (39f) to Eq. (39g) is derived straightforwardly by applying Bayes' theorem.

The two approximations used here are similar to those in [39], with the key difference being the focus on the ETGP in this paper rather than the GP. The rationale behind these approximations is as follows:

- Approximation 1) assumes that the posterior distribution of the latent state at time  $t-1$  based on observations up to  $t-1$  is nearly identical to that based on observations up to  $t$ . This holds particularly well when  $t$  is large, as the additional observation at time  $t$  has minimal impact

$$\mathcal{L} = \mathbb{E}_q \left[ \log \frac{p(\tilde{\mathbf{y}}, \tilde{\mathbf{x}}, \mathbf{w}, \tilde{\mathbf{f}}, \mathbf{u})}{q(\tilde{\mathbf{x}}, \mathbf{w}, \tilde{\mathbf{f}}, \mathbf{u})} \right] \quad (39a)$$

$$= \mathbb{E}_q \left[ \log \frac{p(\tilde{\mathbf{f}}, \mathbf{u})p(\mathbf{w})p(\mathbf{x}_0) \prod_{t=1}^T p(\mathbf{y}_t|\mathbf{x}_t)p(\mathbf{x}_t|\mathbf{w}, \tilde{\mathbf{f}}, \mathbf{x}_{t-1})}{q(\tilde{\mathbf{f}}, \mathbf{u})q(\mathbf{w})q(\mathbf{x}_0) \prod_{t=1}^T q(\mathbf{x}_t|\mathbf{w}, \tilde{\mathbf{f}}, \mathbf{x}_{t-1})} \right] \quad (39b)$$

$$= \mathbb{E}_q \left[ \sum_{t=1}^T \log \frac{p(\mathbf{y}_t, \mathbf{x}_t|\mathbf{w}, \tilde{\mathbf{f}}, \mathbf{x}_{t-1})}{q(\mathbf{x}_t|\mathbf{w}, \tilde{\mathbf{f}}, \mathbf{x}_{t-1})} \right] - \text{KL}(q(\mathbf{u})\|p(\mathbf{u})) - \text{KL}(q(\mathbf{w})\|p(\mathbf{w})) - \text{KL}(q(\mathbf{x}_0)\|p(\mathbf{x}_0)) \quad (39c)$$

$$= \mathbb{E}_q \left[ \sum_{t=1}^T \log \frac{p(\mathbf{y}_t, \mathbf{x}_t|\mathbf{w}, \tilde{\mathbf{f}}, \mathbf{x}_{t-1})p(\mathbf{x}_{t-1}|\mathbf{w}, \tilde{\mathbf{f}}, \mathbf{y}_{1:t-1})}{q(\mathbf{x}_t|\mathbf{w}, \tilde{\mathbf{f}}, \mathbf{x}_{t-1})p(\mathbf{x}_{t-1}|\mathbf{w}, \tilde{\mathbf{f}}, \mathbf{y}_{1:t-1})} \right] - \text{KL}(q(\mathbf{u})\|p(\mathbf{u})) - \text{KL}(q(\mathbf{w})\|p(\mathbf{w})) - \text{KL}(q(\mathbf{x}_0)\|p(\mathbf{x}_0)) \quad (39d)$$

$$\approx \mathbb{E}_q \left[ \sum_{t=1}^T \log \frac{p(\mathbf{y}_t, \mathbf{x}_t|\mathbf{w}, \tilde{\mathbf{f}}, \mathbf{x}_{t-1})p(\mathbf{x}_{t-1}|\mathbf{w}, \tilde{\mathbf{f}}, \mathbf{y}_{1:t-1})}{\underbrace{p(\mathbf{x}_t|\mathbf{w}, \tilde{\mathbf{f}}, \mathbf{x}_{t-1}, \mathbf{y}_{1:t})}_{\text{assumption 1}} \underbrace{p(\mathbf{x}_{t-1}|\mathbf{w}, \tilde{\mathbf{f}}, \mathbf{y}_{1:t})}_{\text{assumption 2}}} \right] - \text{KL}(q(\mathbf{u})\|p(\mathbf{u})) - \text{KL}(q(\mathbf{w})\|p(\mathbf{w})) - \text{KL}(q(\mathbf{x}_0)\|p(\mathbf{x}_0)) \quad (39e)$$

$$= \mathbb{E}_q \left[ \sum_{t=1}^T \log \frac{p(\mathbf{y}_t, \mathbf{x}_t, \mathbf{x}_{t-1}|\mathbf{w}, \tilde{\mathbf{f}}, \mathbf{y}_{1:t-1})}{p(\mathbf{x}_t, \mathbf{x}_{t-1}|\mathbf{w}, \tilde{\mathbf{f}}, \mathbf{y}_{1:t-1}, \mathbf{y}_t)} \right] - \text{KL}(q(\mathbf{u})\|p(\mathbf{u})) - \text{KL}(q(\mathbf{w})\|p(\mathbf{w})) - \text{KL}(q(\mathbf{x}_0)\|p(\mathbf{x}_0)) \quad (39f)$$

$$= \mathbb{E}_{q(\mathbf{w}, \tilde{\mathbf{f}})} \left[ \sum_{t=1}^T \log p(\mathbf{y}_t|\mathbf{y}_{1:t-1}, \mathbf{w}, \tilde{\mathbf{f}}) \right] - \text{KL}(q(\mathbf{u})\|p(\mathbf{u})) - \text{KL}(q(\mathbf{w})\|p(\mathbf{w})) - \text{KL}(q(\mathbf{x}_0)\|p(\mathbf{x}_0)) \quad (39g)$$

on the state estimate due to the accumulated information over time.

- Approximation 2) posits that the variational distribution  $q(\mathbf{x}_t|\mathbf{w}, \tilde{\mathbf{f}}, \mathbf{x}_{t-1})$  is approximated by the filtering distribution  $p(\mathbf{x}_t|\mathbf{w}, \tilde{\mathbf{f}}, \mathbf{x}_{t-1}, \mathbf{y}_{1:t})$ . Note that in variational inference, the variational distribution serves as an approximation of the true smoothing distribution  $p(\mathbf{x}_t|\mathbf{w}, \tilde{\mathbf{f}}, \mathbf{x}_{t-1}, \mathbf{y}_{1:T})$ . While there may be some estimation loss, the approximation is reasonable for long observation sequences where future observations minimally affect state estimates. This trade-off balances accuracy and computational efficiency, a crucial consideration in high-dimensional settings.

## REFERENCES

- [1] S. Särkkä and L. Svensson, *Bayesian filtering and smoothing*. Cambridge university press, 2023, vol. 17.
- [2] A. Kullberg, I. Skog, and G. Hendeby, "Online joint state inference and learning of partially unknown state-space models," *IEEE Trans. Signal Process.*, vol. 69, pp. 4149–4161, 2021.
- [3] U. A. Khan and J. M. Moura, "Distributing the Kalman filter for large-scale systems," *IEEE Trans. Signal Process.*, vol. 56, no. 10, pp. 4919–4935, 2008.
- [4] F. Tobar, P. M. Djurić, and D. P. Mandić, "Unsupervised state-space modeling using reproducing kernels," *IEEE Trans. Signal Process.*, vol. 63, no. 19, pp. 5210–5221, 2015.
- [5] G. Revach, N. Shlezinger, X. Ni, A. L. Escoriza, R. J. Van Sloun, and Y. C. Eldar, "KalmanNet: Neural network aided Kalman filtering for partially known dynamics," *IEEE Trans. Signal Process.*, vol. 70, pp. 1532–1547, 2022.
- [6] A. Ghosh, A. Honoré, and S. Chatterjee, "DANSE: Data-driven non-linear state estimation of model-free process in unsupervised learning setup," *IEEE Trans. Signal Process.*, pp. 1824–1838, 2024.
- [7] L. Girin, S. Leglaive, X. Bie, J. Diard, T. Hueber, and X. Alameddine, "Dynamical variational autoencoders: A comprehensive review," *Found. Trends Mach. Learn.*, vol. 15, no. 1-2, pp. 1–175, 2021.
- [8] R. Krishnan, U. Shalit, and D. Sontag, "Structured inference networks for nonlinear state space models," in *Proc. AAAI Conf. Artif. Intell. (AAAI)*, 2017, pp. 2101–2109.
- [9] A. M. Alaa and M. van der Schaar, "Attentive state-space modeling of disease progression," in *Proc. Adv. Neural Inf. Process. Syst. (NeurIPS)*, 2019, pp. 11 338–11 348.
- [10] C. M. Bishop, *Pattern Recognition and Machine Learning*. Springer, 2006.
- [11] C. E. Rasmussen and C. K. I. Williams, *Gaussian Processes for Machine Learning*. MIT Press, 2006.
- [12] R. Frigola, "Bayesian time series learning with Gaussian processes," Ph.D. dissertation, University of Cambridge, 2015.
- [13] J. M. Wang, D. J. Fleet, and A. Hertzmann, "Gaussian process dynamical models for human motion," *IEEE Trans. Pattern Anal. Mach. Intell.*, vol. 30, no. 2, pp. 283–298, 2007.
- [14] M. P. Deisenroth, D. Fox, and C. E. Rasmussen, "Gaussian processes for data-efficient learning in robotics and control," *IEEE Trans. Pattern Anal. Mach. Intell.*, vol. 37, no. 2, pp. 408–423, 2013.
- [15] K. Arulkumaran, M. P. Deisenroth, M. Brundage, and A. A. Bharath, "Deep reinforcement learning: A brief survey," *IEEE Signal Process. Mag.*, vol. 34, no. 6, pp. 26–38, 2017.
- [16] Z. Yan, P. Cheng, Z. Chen, Y. Li, and B. Vucetic, "Gaussian process reinforcement learning for fast opportunistic spectrum access," *IEEE Trans. Signal Process.*, vol. 68, pp. 2613–2628, 2020.
- [17] A. Xie, F. Yin, B. Ai, S. Zhang, and S. Cui, "Learning while tracking: A practical system based on variational Gaussian process state-space model and smartphone sensory data," in *Proc. Int. Conf. Inf. Fusion (FUSION)*, 2020, pp. 1–7.
- [18] K. Berntorp and M. Menner, "Constrained Gaussian-process state-space models for online magnetic-field estimation," in *Proc. Int. Conf. Inf. Fusion (FUSION)*, 2023, pp. 1–7.
- [19] J. Ko and D. Fox, "GP-BayesFilters: Bayesian filtering using Gaussian process prediction and observation models," *Auton. Robots*, vol. 27, no. 1, pp. 75–90, 2009.
- [20] M. P. Deisenroth, M. F. Huber, and U. D. Hanebeck, "Analytic moment-based Gaussian process filtering," in *Proc. Int. Conf. Mach. Learn. (ICML)*, 2009, pp. 225–232.
- [21] M. P. Deisenroth, R. D. Turner, M. F. Huber, U. D. Hanebeck, and C. E. Rasmussen, "Robust filtering and smoothing with Gaussian processes," *IEEE Trans. Autom. Control*, vol. 57, no. 7, pp. 1865–1871, 2011.

- [22] J. Ko and D. Fox, "Learning GP-BayesFilters via Gaussian process latent variable models," *Auton. Robots*, vol. 30, no. 1, pp. 3–23, 2011.
- [23] R. Frigola, F. Lindsten, T. B. Schön, and C. E. Rasmussen, "Bayesian inference and learning in Gaussian process state-space models with particle MCMC," in *Proc. Adv. Neural Inf. Process. Syst. (NeurIPS)*, 2013, pp. 3156–3164.
- [24] A. Svensson, A. Solin, S. Särkkä, and T. Schön, "Computationally efficient Bayesian learning of Gaussian process state space models," in *Proc. Int. Conf. Artif. Intell. Stat. (AISTATS)*, 2016, pp. 213–221.
- [25] A. Svensson and T. B. Schön, "A flexible state–space model for learning nonlinear dynamical systems," *Automatica*, vol. 80, pp. 189–199, 2017.
- [26] K. Berntorp, "Online Bayesian inference and learning of Gaussian-process state–space models," *Automatica*, vol. 129, p. 109613, 2021.
- [27] Y. Liu, M. Ajirak, and P. M. Djurić, "Sequential estimation of Gaussian process-based deep state-space models," *IEEE Trans. Signal Process.*, vol. 71, pp. 2968–2980, 2023.
- [28] A. Solin and S. Särkkä, "Hilbert space methods for reduced-rank Gaussian process regression," *Stat. Comput.*, vol. 30, no. 2, pp. 419–446, 2020.
- [29] R. Frigola, Y. Chen, and C. E. Rasmussen, "Variational Gaussian process state-space models," in *Proc. Adv. Neural Inf. Process. Syst. (NeurIPS)*, 2014, pp. 3680–3688.
- [30] A. J. McHutchon, "Nonlinear modelling and control using Gaussian processes," Ph.D. dissertation, University of Cambridge, 2014.
- [31] S. Eleftheriadis, T. Nicholson, M. P. Deisenroth, and J. Hensman, "Identification of Gaussian process state space models," in *Proc. Adv. Neural Inf. Process. Syst. (NeurIPS)*, 2017, pp. 5309–5319.
- [32] A. Doerr, C. Daniel, M. Schiegg, N.-T. Duy, S. Schaal, M. Toussaint, and T. Sebastian, "Probabilistic recurrent state-space models," in *Proc. Int. Conf. Mach. Learn. (ICML)*, 2018, pp. 1280–1289.
- [33] A. D. Ialongo, M. van der Wilk, J. Hensman, and C. E. Rasmussen, "Overcoming mean-field approximations in recurrent Gaussian process models," in *Proc. Int. Conf. Mach. Learn. (ICML)*, 2019, pp. 2931–2940.
- [34] S. Curi, S. Melchior, F. Berkenkamp, and A. Krause, "Structured variational inference in partially observable unstable Gaussian process state space models," in *Proc. Learning for Dynamics and Control (LADC)*, 2020, pp. 147–157.
- [35] Y. Liu and P. M. Djurić, "Gaussian process state-space models with time-varying parameters and inducing points," in *Proc. European Signal Process. Conf. (EUSIPCO)*, 2021, pp. 1462–1466.
- [36] J. Lindinger, B. Rakitsch, and C. Lippert, "Laplace approximated Gaussian process state-space models," in *Proc. Conf. Uncertain. Artif. Intell. (UAI)*, vol. 180, 2022, pp. 1199–1209.
- [37] X. Fan, E. V. Bonilla, T. O’Kane, and S. A. Sisson, "Free-form variational inference for Gaussian process state-space models," in *Proc. Int. Conf. Mach. Learn. (ICML)*, 2023, pp. 9603–9622.
- [38] Z. Lin, F. Yin, and J. Maroñas, "Towards flexibility and interpretability of Gaussian process state-space model," *arXiv preprint arXiv:2301.08843*, 2023.
- [39] Z. Lin, Y. Sun, F. Yin, and A. Thiéry, "Ensemble Kalman filtering meets Gaussian process SSM for non-mean-field and online inference," *IEEE Trans. Signal Process.*, vol. 72, pp. 4286–4301, Aug. 2024.
- [40] Z. Lin, J. Maroñas, Y. Li, F. Yin, and S. Theodoridis, "Towards efficient modeling and inference in multi-dimensional Gaussian process state-space models," in *Proc. IEEE Int. Conf. Acoust. Speech Signal Process. (ICASSP)*, 2024, pp. 12 881–12 885.
- [41] Z. Lin, L. Cheng, F. Yin, L. Xu, and S. Cui, "Output-dependent Gaussian process state-space model," in *Proc. IEEE Int. Conf. Acoust. Speech Signal Process. (ICASSP)*, 2023, pp. 1–5.
- [42] M. Titsias, "Variational learning of inducing variables in sparse Gaussian processes," in *Proc. Int. Conf. Artif. Intell. Stat. (AISTATS)*, 2009, pp. 567–574.
- [43] J. Hensman, N. Fusi, and N. D. Lawrence, "Gaussian processes for big data," in *Proc. Conf. Uncertain. Artif. Intell. (UAI)*, 2013, pp. 282–290.
- [44] C. Ma, Y. Li, and J. M. Hernández-Lobato, "Variational implicit processes," in *Proc. Int. Conf. Mach. Learn. (ICML)*, 2019, pp. 4222–4233.
- [45] I. Kobyzev, S. J. Prince, and M. A. Brubaker, "Normalizing flows: An introduction and review of current methods," *IEEE Trans. Pattern Anal. Mach. Intell.*, vol. 43, no. 11, pp. 3964–3979, 2020.
- [46] K. Chen, T. van Laarhoven, E. Marchiori, F. Yin, and S. Cui, "Multitask Gaussian process with hierarchical latent interactions," in *Proc. IEEE Int. Conf. Acoust., Speech, Signal Process Proc. (ICASSP)*, 2022, pp. 4148–4152.
- [47] J. Maroñas, O. Hamelijnck, J. Knoblauch, and T. Damoulas, "Transforming Gaussian processes with normalizing flows," in *Proc. Int. Conf. Artif. Intell. Stat. (AISTATS)*, 2021, pp. 1081–1089.
- [48] G. Rios and F. Tobar, "Compositionally-warped Gaussian processes," *Neural Netw.*, vol. 118, pp. 235–246, Oct. 2019.
- [49] L. Dinh and S. Bengio, "Density estimation using Real NVP," in *Proc. Int. Conf. Learn. Represent. (ICLR)*, 2017.
- [50] J. Maroñas and D. Hernández-Lobato, "Efficient transformed Gaussian processes for non-stationary dependent multi-class classification," in *Proc. Int. Conf. Mach. Learn. (ICML)*, 2023, pp. 24 045–24 081.
- [51] A. Gu and T. Dao, "Mamba: Linear-time sequence modeling with selective state spaces," in *Proc. First Conference on Language Modeling*, Oct. 2024.
- [52] S. Theodoridis, *Machine Learning: A Bayesian and Optimization Perspective*, 2nd ed. Academic Press, 2020.
- [53] M. Titsias and N. D. Lawrence, "Bayesian Gaussian process latent variable model," in *Proc. Int. Conf. Artif. Intell. Stat. (AISTATS)*. JMLR Workshop and Conference Proceedings, 2010, pp. 844–851.
- [54] A. Damianou and N. D. Lawrence, "Deep Gaussian processes," in *Proc. Int. Conf. Artif. Intell. Stat. (AISTATS)*, 2013, pp. 207–215.
- [55] G. Evensen, "Sequential data assimilation with a nonlinear quasi-geostrophic model using Monte Carlo methods to forecast error statistics," *J. Geophys. Res. Oceans*, vol. 99, no. C5, pp. 10 143–10 162, 1994.
- [56] Y. Chen, D. Sanz-Alonso, and R. Willett, "Autodifferentiable ensemble Kalman filters," *SIAM J. Math. Data Sci.*, vol. 4, no. 2, pp. 801–833, 2022.
- [57] D. P. Kingma and M. Welling, "An introduction to variational autoencoders," *Found. Trends Mach. Learn.*, vol. 12, no. 4, pp. 307–392, 2019.
- [58] A. Paszke, S. Gross, F. Massa, A. Lerer, J. Bradbury, G. Chanan, T. Killeen, Z. Lin, N. Gimelshein, L. Antiga *et al.*, "Pytorch: an imperative style, high-performance deep learning library," in *Proc. Adv. Neural Inf. Process. Syst. (NeurIPS)*, 2019, pp. 8026–8037.
- [59] D. P. Kingma and J. Ba, "Adam: A method for stochastic optimization," in *Proc. Int. Conf. Learn. Represent. (ICLR)*, 2015.
- [60] E. N. Lorenz, "Predictability: A problem partly solved," in *Proc. Seminar on predictability*, vol. 1, no. 1. Reading, 1996, pp. 1–18.